Water Resour Manage
https://doi.org/10.1007/s11269-018-1949-x

# Effects of Global Warming on Precipitation Extremes: Dependence on Storm Characteristics

**Abhishek Gaur**[1] · **Andre Schardong**[2] · **Slobodan Simonovic**[2]

Received: 18 July 2017 / Accepted: 23 February 2018


**Abstract** This study investigates the relationship between historically observed changes in extreme precipitation magnitudes and temperature ($P_{ex}$-T relationship) at multiple locations in Canada. The focus is on understanding the behavior of these relationships with regards to key storm characteristics such as its duration, season of occurrence, and location. To do so, three locations are chosen such that they have large amounts of moisture available near them whereas four locations are chosen such that they are located in the land-locked regions of Canada and subsequently have no nearby moisture source available on them. To investigate the effect of different storm durations on $P_{ex}$-T relationship, storms of durations: 5, 10, 15, 30 min, 1, 2, 6, 12, 24 h are considered. Finally, $P_{ex}$-T relationship is analyzed separately for summer and winter seasons to quantify the influence of seasons. Results indicate strong influences of storm duration, season of occurrence, and location on observed precipitation scaling rates. Drastic intensification of precipitation extremes with temperature is obtained for shorter duration precipitation events than for longer duration precipitation events, in summers than in the winters. Furthermore, in summertime, increases in the intensity of convection driven precipitation extremes is found highest at locations away from large waterbodies. On the other hand, in wintertime most drastic increases in extreme precipitation are obtained at locations near large waterbodies. These findings contribute towards increasing the current understanding of precipitation extremes in the context of rapidly increasing global temperatures.

**Keywords** Clausius-Clapeyron · Precipitation extremes · Temperature · Storm duration · Moisture availability

**Electronic supplementary material** The online version of this article (https://doi.org/10.1007/s11269-018-1949-x) contains supplementary material, which is available to authorized users.

✉ Abhishek Gaur
abhishek.gaur1988@gmail.com

[1] National Research Council Canada, 1200 Montreal Road, Ottawa, ON K1A0R6, Canada

[2] Facility for Intelligent Decision Support, Department of Civil and Environmental Engineering, Western University, London, ON N6A 3K7, Canada

Published online: 12 March 2018

## 1 Introduction

Human induced climate change is expected to bring considerable changes in hydro-climatic regimes across the globe (Stocker et al. 2013). Global Climate Models (GCMs) have been used to simulate future climatic conditions under projected future greenhouse gas trajectories. The skills of GCMs rely heavily on their ability to simulate complex geo-physical and chemical processes occurring within the global climate system. While some of these processes such as energy balance are well represented in the GCMs, some other such as convection, are highly simplified. Due to such inadequacies in simulating key physical processes, GCMs have been found to exhibit more skill in modelling temperatures than precipitation (Stocker et al. 2013).

An increase in temperature across the globe is the most robust climatic change projected by GCMs over the twenty-first century. Precipitation extremes are expected to become more intense in warmer future climate following the Clausius-Clapeyron (C-C) relationship. The C-C relationship expresses the saturation water vapor pressure ($e_s$) as a function of absolute atmospheric temperature (T) as:

$$\frac{\partial e_s}{\partial T} = \frac{l_v e_s}{R_v T^2} \tag{1}$$

where, $l_v$ is the latent heat of vaporization and $R_v$ is the gas constant. Upon simplification and incorporation of theoretical values of the atmospheric constants, above relationship describes saturation-specific humidity to follow an exponential curve and increase with temperature at a scaling rate of ~7% per °C. This scaling in saturation-specific humidity translates to an increase in the magnitude of extreme precipitation events in conditions when relative humidity stays constant (Westra et al. 2014). This precipitation scaling rate of ~7% per °C is referred as the 'theoretical' precipitation scaling rate (PSR) in the rest of the paper.

Given that temperature projections made by the GCMs are reliable and robust, the prospect of using C-C relationship to estimate future precipitation extremes has resulted in the evaluation of extreme precipitation-temperature relationship and quantification of PSR in many studies (Zhang et al. 2017a, b; Wasko et al. 2016; Miao et al. 2016; Drobinski et al. 2016; Molnar et al. 2015; Panthou et al. 2014; Westra et al. 2013; Lenderink and Meijgaard 2008). Different indices including temperature specific precipitation extremes (Drobinski et al. 2016; Lenderink and Meijgaard 2008), precipitation events crossing 95th quantile (Zhang et al. 2017a, b; Scoccimarro et al. 2015), precipitation events crossing 98th quantile (Wasko and Sharma 2014), precipitation events crossing 99th quantile (Shaw et al. 2011) and annual maximum precipitation (Westra et al. 2013) have been used to define precipitation extremes when calculating PSRs. Zhang et al. (2017a) demonstrates that the magnitude of calculated ('observed' hereafter) PSRs depend critically on the methodology chosen to extract extreme precipitation quantiles.

Molnar et al. (2015) compared the observed PSR magnitudes of convection driven precipitation events with non-convection driven events. They obtained higher PSR magnitudes for the former storm types than the latter. Similar findings have been made in other studies (Berg and Haerter 2013). In addition, the duration of the storm event (Haerter et al. 2010; Zhang et al. 2017b), season of occurrence (Berg et al. 2009; Shaw et al. 2011), and location (Panthou et al. 2014) have been identified as factors shaping the spatio-temporal variability of PSR magnitudes.

The objective of this study to analyze the variation of PSR magnitudes with key precipitation storm characteristics such as its season of occurrence, its duration, and its location with reference to nearby moisture sources. Different extreme precipitation thresholds are also used to define extremes and the sensitivity of PSR magnitudes towards the selected thresholds are also analyzed. Since similar assessments (as reviewed before) have been performed mostly in Europe, this study is among the few studies (such as Panthou et al. 2014) that have assessed the spatio-temporal variability of PSR magnitudes in Canada. Additionally, many previous assessments (including Panthou et al. 2014) have used a temperature-bin based approach (Lenderink and Meijgaard 2008) to obtain the PSR magnitudes. Recently, limitations of such an approach have been identified and a trend based approach to estimate PSR magnitudes have been recommended in Zhang et al. (2017a). Therefore, in this study, we have adopted a trend based approach to assess the spatio-temporal variability of PSR magnitudes at different locations in Canada.

The rest of the paper is organized as follows. Study region is described in section 2. Data and methods used in this study are explained in section 3, followed by details of analysis performed and results obtained in section 4. Finally, conclusions based on the obtained results and related discussions are provided in section 5.

## 2 Study region

In this study seven locations are chosen for the investigation of precipitation scaling rates. A list of the selected locations is provided in Table 1 and their distribution is presented in Fig. 1. To investigate the influence of immediate moisture availability on precipitation scaling, three out of the seven chosen locations: LON, MON, VAN, are chosen close to large water-bodies. Among them, LON is surrounded by the Great Lakes, while MON and VAN are surrounded by the Atlantic and Pacific oceans respectively. Remaining four locations: BRN, WEY, IND, KIN are chosen so that they are away from large water-bodies. All these four locations are located in the land-locked prairies region of Canada. The selection of chosen locations is also guided by the length of continuous 5 min precipitation data available at tipping bucket rain gauge (TBRG) stations across Canada. Locations with longer continuous data-records are given preference over locations where shorter data-lengths are available.

**Table 1** Details of the locations considered for analysis in this study

| S.No | Location | Short-name | Longitude (°E) | Latitude (°N) | Period of data availability |
|---|---|---|---|---|---|
| 1 | London | LON | −81.2 | 43.0 | 1943–2007 |
| 2 | Moncton | MON | −64.7 | 46.1 | 1960–2014 |
| 3 | Brandon | BRN | −99.9 | 49.9 | 1970–2013 |
| 4 | Vancouver | VAN | −123.2 | 49.2 | 1960–2013 |
| 5 | Weyburn | WEY | −103.8 | 49.7 | 1961–2007 |
| 6 | Indian Head CDA | IND | −103.7 | 50.6 | 1962–1995 |
| 7 | Kindersley A | KIN | −109.2 | 51.5 | 1984–2013 |

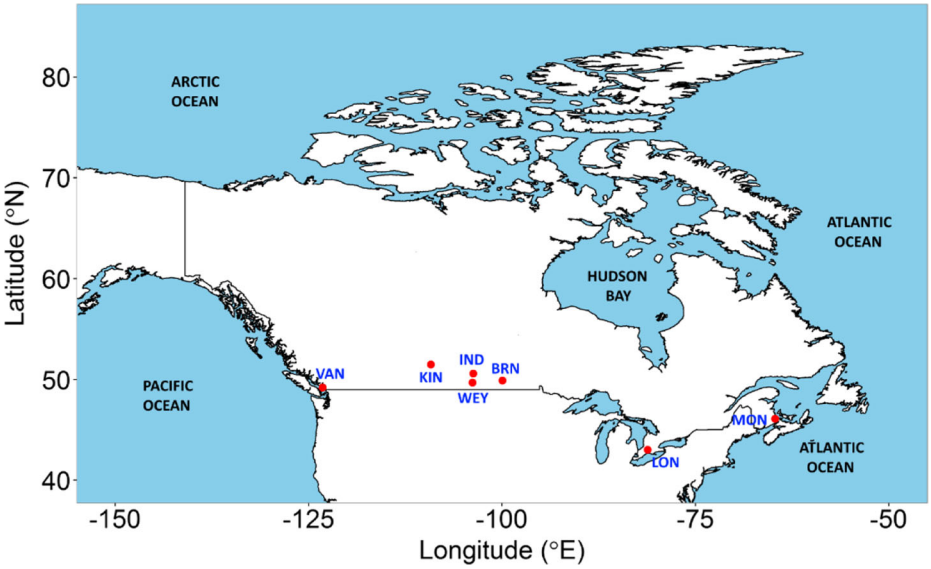


**Fig. 1** Locations analyzed in this study

## 3 Data and Methodology

Five minute frequency precipitation and daily mean temperatures data are collected for the seven locations from Environment and Climate Change Canada (ECCC). These data are then used to derive precipitation scaling rates using following steps:

- Five minute frequency precipitation data are used to obtain daily 5, 10, 15, 30 min, 1, 2, 6, 12, 24 h precipitation maximum series.
- Observed precipitation rates are derived using the C-C relationship that describes that natural logarithm of extreme precipitation magnitude varies systematically with temperature at an observed scaling rate. In this study, PSRs are estimated separately for summer (May to October) and winter (November to April) months.
- Multiple approaches for defining and selecting precipitation extremes are considered. Chosen approaches extract annual maximum precipitation (a-max), and precipitation events above multiple quantile thresholds for analysis. Methods considering precipitation exceeding 80th, 90th, 95th, 97th, 98th, and 99th quantile for the estimation of scaling rates are referred as q80, q85, q90, q95, q97, q98, and q99 respectively hereafter.
- The relationship between extreme precipitation and temperature is modelled by assuming that it follows the Clausius-Clapeyron relationship i.e. by considering that natural log of extreme precipitation varies linearly with temperature. Median regression, as opposed to least squared regression, is used to link log of extreme precipitation with temperature as former has been found to be more robust to outliers as compared to the latter (Koenker and Hallock 2001). The mathematical formulation of the modelled relationship can be presented as:

$$\ln(P_{ex})^q = \beta_0{}^q + \beta_1{}^q \times T_{mean} + \varepsilon^q \quad (2)$$

where, $P_{ex}$ denotes the magnitude of extreme precipitation, $T_{mean}$ represents the daily mean temperature of the day of the occurrence of precipitation extreme, $\beta_0{}^q$ is the quantile specific intercept parameter, $\beta_1{}^q$ is the quantile specific slope parameter (or PSR), and $\varepsilon^q$ is the quantile specific error component of the model. The magnitude and statistical significance of PSRs at $p = 0.05$ is recorded for further analysis.

## 4 Results

The PSR magnitudes obtained during summers at locations near (far away from) large waterbodies are summarized in Table 2 (Table 3). Corresponding results for winters are summarized in Table 4 (Table 5).

Largest numbers (47%) of statistically significant PSRs are obtained when precipitation events above 80th quantile are considered as extremes, followed by q85 (42%), q90 (37%), q95 (22%), a-max (13%), q97 (10%), q98 (3%), and q99 (2%). Highest PSR magnitudes are obtained when a-max is considered to estimate scaling rates, followed by q80 and q85, followed by q90, q97, q95, q98, and q99.

**Table 2** Precipitation scaling rates obtained in summertime at locations near large waterbodies

| Location | Method | 5m | 10m | 15m | 30m | 1h | 2h | 6h | 12h | 24h |
|---|---|---|---|---|---|---|---|---|---|---|
| LON | a-max | 1.4 | 1.8 | -1.1 | -2.3 | 0.7 | 2.4 | 2.0 | 1.1 | 2.2* |
| | q80 | 3.2* | 3.6* | 2.7* | 3.0* | 2.2* | 2.1* | 1.1* | 1.3* | 0.9* |
| | q85 | 2.4* | 2.6* | 2.4* | 2.1* | 2.2* | 1.5* | 1.4* | 1.1* | 1.4* |
| | q90 | 0.7 | 1.3* | 1.6* | 1.9* | 1.3* | 1.4* | 1.5* | 1.3* | 1.0* |
| | q95 | 0.3 | 1.6* | 0.8 | -0.2 | 0.5 | 0.4 | 0.6 | 0.3 | 0.3 |
| | q97 | 0.8 | -0.3 | -0.1 | 0.9 | 1.0 | 1.6 | 1.3* | 1.1* | 1.0 |
| | q98 | 1.2 | 0.3 | -0.6 | -0.2 | -2.0 | -0.2 | 1.0 | 0.5 | 0.2 |
| | q99 | -0.7 | -4.1 | 0 | -0.3 | 0.5 | -0.6 | 0 | -0.3 | 0.7 |
| MON | a-max | 3.6 | 4.3* | 5.6* | 0.2 | 2.0 | 1.9 | 1.9 | 2.0 | 1.9 |
| | q80 | 3.2* | 3.0* | 2.8* | 2.3* | 1.5* | 1.2* | 0.7* | -0.2 | -0.3 |
| | q85 | 3.3* | 3.2* | 2.6* | 1.6* | 1.7* | 1.5* | 0.8 | 0.1 | 0.2 |
| | q90 | 3.0* | 2.1* | 1.5* | 1.0 | 1.5* | 1.6* | 0.6 | 0.2 | 0.5 |
| | q95 | 2.1* | 1.2* | 1.9* | 1.0* | 0.9 | -0.2 | 1.5* | 1.2* | -0.2 |
| | q97 | 1.8* | 0.8* | 1.4 | 1.9* | -0.2 | -1.1 | 0.9 | 0.6 | 0.7 |
| | q98 | -1.4 | 0.7 | 1.0 | 0.1 | 0.2 | -0.5 | -0.7 | 0.5 | 1.1 |
| | q99 | -1.0 | 0.3 | 0 | -0.6 | 1.1 | 0.7 | -0.2 | -0.1 | -1.3* |
| VAN | a-max | 6.4* | 3.3 | 4.8 | 5.6 | 2.3 | 2.6 | -0.6 | -0.4 | -0.3 |
| | q80 | 1.3* | 2.2* | 1.5* | 1.4* | 0.4 | -1.3* | -0.6 | -1.5* | -1.4* |
| | q85 | 2.1* | 2.8* | 2.2* | 1.3* | 0.7 | -0.5 | -0.5 | -1.5* | -0.6 |
| | q90 | 1.1 | 2.1* | 1.6* | 1.0 | 0.6 | 0.7 | -1.0 | 0.1 | -0.3 |
| | q95 | 0.9 | 0.3 | 1.3 | 1.4* | 0.3 | 1.2 | -0.7 | -0.6 | -0.1 |
| | q97 | 2.7 | 0.6 | -2.1 | -1.3 | 1.7 | 0.3 | 0.5 | -0.4 | 0.5 |
| | q98 | 1.5 | 2.5 | 2.4 | -2.6 | 1.8 | 0.4 | -1.2 | -1.0 | -0.7 |
| | q99 | 1.0 | -1.4 | -0.7 | -0.1 | 1.2 | 1.2 | 0.3 | -1.8 | -1.2 |

Statistically significant scaling rates (at $p = 0.05$) are marked with an asterisk (*) sign. Cells filled with dark and light blue (orange) colors are associated with statistically significant and statistically insignificant positive (negative) scaling rates respectively

**Table 3** Precipitation scaling rates obtained in summertime at locations away from large waterbodies

| Location | Method | 5m | 10m | 15m | 30m | 1h | 2h | 6h | 12h | 24h |
|---|---|---|---|---|---|---|---|---|---|---|
| BRN | a-max | 2.8 | 4.9 | 4.3 | 5.2 | 7.2* | 6.8* | 5.3* | 3.7 | 3.9 |
| | q80 | 4.6* | 3.3* | 3.3* | 3.0* | 2.8* | 2.6* | 0.7 | 0.4 | 0.5 |
| | q85 | 2.8* | 3.1* | 2.0* | 2.1* | 2.9* | 2.9* | 1.1 | 0.9 | 1.5* |
| | q90 | 1.6* | 1.5 | 2.8* | 2.2* | 2.7* | 2.3* | 1.6* | 0.7 | 1.7* |
| | q95 | 1.3 | 1.4 | 2.3* | 4.0* | 3.6* | 2.9* | 1.0 | 1.4 | 0.6 |
| | q97 | 1.7 | 0.5 | 0.9 | 0.8 | 0.5 | 1.4* | 1.2 | 0.9 | 0.4 |
| | q98 | -1.1 | 1.4 | 1.3 | -0.8 | 1.3 | 0.3 | 0.8 | 0.2 | 1.4 |
| | q99 | 2.4 | -0.3 | -0.1 | 0 | -2.1 | 1.0 | 0.2 | 1.3 | 1.7* |
| KIN | a-max | 11.1* | 2.9 | 1.5 | 5.6 | 5.4* | 7.7 | 0.9 | 2.5 | 0.4 |
| | q80 | 3.3* | 3.2* | 3.9* | 3.6* | 3.4* | 3.4* | 0.7 | 1.7* | 0.9 |
| | q85 | 3.3* | 4.1* | 3.1* | 4.1* | 3.3* | 2.2* | 1.7* | 1.0 | 0.9 |
| | q90 | 1.6 | 3.1 | 4.4* | 4.1* | 2.1* | 1.3 | 1.3 | 1.2 | 0.2 |
| | q95 | 3.7* | 3.5* | 2.4 | 2.5 | 1.1 | 2.3* | 0.9 | 2.4* | -0.2 |
| | q97 | 1.9 | 2.6 | 2.5 | 3.3 | 2.5 | 1.5 | 0.4 | -1.5 | 1.6 |
| | q98 | 1.8 | 2.3* | 0.8 | 1.0 | 0.7 | 3.6 | 1.4 | -0.7 | 0.5 |
| | q99 | -2.1 | -0.6 | -0.7 | 1.0 | 1.8 | 0 | -0.3 | 1.3 | 0.1 |
| IND | a-max | 7.2* | 6.8* | 7.1* | 7.3* | 3.6 | 4.3 | 3.9 | 1.7 | 1.4 |
| | q80 | 3.1* | 4.2* | 4.3* | 2.9* | 1.9* | 2.4* | 1.0 | 0.3 | -0.8 |
| | q85 | 1.9* | 3.4* | 3.0* | 3.2* | 2.9* | 1.9* | 0.7 | -0.4 | 0 |
| | q90 | 2.5* | 2.7* | 2.6* | 3.1* | 2.5* | 2.1* | 1.0 | -0.5 | -0.7 |
| | q95 | 2.4* | 2.0 | -0.5 | 1.6 | 2.2* | 1.3 | -0.1 | 0.1 | 0.2 |
| | q97 | 2.1* | 1.6 | 2.2 | 3.0 | 1.8 | 0.4 | 0.1 | -0.1 | 0.7 |
| | q98 | -0.8 | 2.2 | 2.4 | 0.8 | -0.6 | 1.1 | -0.7 | 1.2 | 1.1 |
| | q99 | 4.8 | 3.0 | -1.0 | -1.9 | 3.6 | 0.2 | 1.5 | -0.8 | 0.4 |
| WEY | a-max | 2.6 | 4.1 | 2.8 | 4.7 | 1.2 | 2.9 | 3.0 | -0.7 | -1.5 |
| | q80 | 3.9* | 3.6* | 2.5* | 2.3* | 1.6* | 1.6* | 0.2 | -0.3 | 0.2 |
| | q85 | 3.0* | 2.6* | 3.0* | 2.9* | 2.6* | 0.9 | 1.3 | 0.3 | -0.1 |
| | q90 | 0.9 | 2.6* | 3.3* | 2.5* | 1.4 | 1.6* | 0.2 | 0.3 | 0.1 |
| | q95 | -0.2 | 1.1 | 0.1 | 1.7 | 1.9* | 1.9* | -0.2 | -0.6 | 0.2 |
| | q97 | 0.4 | -0.1 | -2.4 | 0.1 | -0.8 | 1.5 | 1.1 | -0.6 | 0.4 |
| | q98 | -0.4 | -1.3 | -0.9 | 0.9 | 0 | -1.8 | 2.1 | -0.7 | 0 |
| | q99 | -0.2 | -1.4 | 1.6 | 1.4 | -1.8 | 0 | 0.5 | 0.4 | 0.1 |

Statistically significant scaling rates (at $p = 0.05$) are marked with an asterisk (*) sign. Cells filled with dark and light blue (orange) colors are associated with statistically significant and statistically insignificant positive (negative) scaling rates respectively

Between the two seasons, a total of 33% of all cases analyzed are found to be associated with a statistically significant increasing scaling rate in summers. On the other hand, only 10% such cases are obtained. A comparison of the magnitudes of scaling rates between summer and winter seasons also indicates similar findings. Considering all precipitation extreme selection methods, a median precipitation scaling rate of 1.2% per °C is obtained in the summers and 0.5% per °C is obtained in winters. These findings indicate more drastic scaling of precipitation extremes with temperature increases during the summer months than during the winter months.

PSR magnitudes and their variations are also found different for stations located near vs. away from large waterbodies. Larger PSR magnitudes are obtained at locations away from large waterbodies than locations near large waterbodies during the summers whereas reverse observations are made during the winters. Considering all precipitation durations, a median PSR of 1.5% (0.1%) per °C is obtained in the summers (winters) at locations away from large waterbodies whereas a median precipitation scaling rate of 0.9% (0.7%) per °C is obtained in the summers (winters) at locations near large waterbodies.

**Table 4** Precipitation scaling rates obtained in wintertime at locations near large waterbodies

| Station | Method | 5m | 10m | 15m | 30m | 1h | 2h | 6h | 12h | 24h |
|---|---|---|---|---|---|---|---|---|---|---|
| LON | a-max | 2.0 | 1.4 | 2.4 | 0.2 | 0.7 | -1.1 | 0.7 | -1.8 | -1.3 |
| | q80 | 1.7* | 2.4* | 1.5* | 1.4* | 1.1* | 1.0 | 0.5 | 0.6 | 0.9 |
| | q85 | 2.1* | 2.2* | 1.7* | 1.4* | 0.7 | 0.7 | 0.4 | 0.6 | 0.6 |
| | q90 | 1.2* | 1.3* | 1.3* | 1.3* | 0.8 | 0.9* | 0.2 | 0.1 | -1.0 |
| | q95 | 1.2* | 0.7 | 0.9 | -0.4 | 1.2* | -0.2 | -0.6 | -0.6 | -1.3 |
| | q97 | 0.3 | 1.0 | 1.3 | 1.4* | 0 | 1.6* | -0.4 | 0 | 0.8 |
| | q98 | 0.8 | -0.6 | 0.4 | 1.4* | 1.0 | 1.2* | 0.5 | -1.0 | 0.1 |
| | q99 | 1.1 | -0.6 | -1.6 | 1.1 | 1.8 | -0.6 | 1.1 | -0.1 | -0.3 |
| MON | a-max | 2.0 | 1.9 | 2.4 | 1.4 | 1.6 | 0.6 | 0.1 | -0.4 | 1.1 |
| | q80 | 0.8* | 0.7* | 0.5 | 0.6 | 0.2 | 0.5 | -0.7 | -0.1 | 0.5 |
| | q85 | 0.8 | 0.4 | 0.7 | 0.5 | 0.4 | 0.6 | -0.4 | -0.1 | 0.5 |
| | q90 | 0.5 | 1.0 | 1.0* | 0.9* | 0.5 | 0.1 | 0.4 | 0.6 | 0.6 |
| | q95 | 0.7 | 1.2* | 0.8 | 0.8* | 0.8 | 0.4 | 0.5 | -0.1 | 0.6 |
| | q97 | 0.2 | 0.8 | 0.8 | 1.0 | 0.4 | -0.1 | 0 | 0.5 | 1.5* |
| | q98 | 0.8 | 0.7 | 0.9 | 1.0 | 0.5 | -0.2 | 0.4 | 0.3 | 0.1 |
| | q99 | 1.4 | 0.7 | 1.0 | 0.7 | 0.8 | -0.2 | 0.6 | 1.3 | -1.0 |
| VAN | a-max | 6.0* | 5.7* | 3.6* | 1.1 | 1.5 | 1.6 | -1.3 | -0.2 | 0.2 |
| | q80 | 1.8* | 1.2* | 6.7 | 1.4* | 0.7 | 0.3 | -0.1 | -0.1 | 0.3 |
| | q85 | 1.9* | 1.8* | 0.7 | 1.1* | 0.4 | 0.8 | 0.3 | -0.3 | 0 |
| | q90 | 2.3* | 1.6* | 1.7* | 0.9* | 0.5 | 0.4 | 0.1 | -0.3 | 0.5 |
| | q95 | 1.8* | 1.3* | 1.1* | 1.1* | 0.2 | 0.4 | 0.1 | 0.5 | 0.6 |
| | q97 | 1.8* | 2.1* | 1.6 | 0.9 | -0.6 | 0.5 | 0.1 | -0.5 | -0.4 |
| | q98 | 1.3 | 1.7 | 1.3 | 1.2* | 0.7 | 0.3 | 0 | 0 | 0 |
| | q99 | 1.9 | 2.1 | 0.9 | 0.9 | 0.8 | 1.2 | 0.1 | -0.4 | 0.6 |

Statistically significant scaling rates (at $p = 0.05$) are marked with an asterisk (*) sign. Cells filled with dark and light blue (orange) colors are associated with statistically significant and statistically insignificant positive (negative) scaling rates respectively

Precipitation rates are found to systematically vary with the duration of extreme precipitation event. In general, higher precipitation scaling rates are obtained for shorter duration precipitation events as compared to longer duration precipitation events. This can be noted from Figure S1 where variation of summertime and wintertime precipitation scaling rates with precipitation duration is presented for stations away and near large waterbodies. Bold blue line joins the median scaling rates associated with precipitation of different durations. A decreasing trend in median scaling rates can be clearly noted in all seasons except in the case of wintertime precipitation at locations away from large waterbodies.

Finally, it is noted that the scaling rates obtained are lower than the theoretical scaling rate of 7% per °C especially during winters. This can be noted from Table S1 where median PSR values are summarized for summer and winter seasons. Median of all PSR values is provided under the column 'all' whereas median of statistically significant values are provided under the column 'sig'.

## 5 Conclusions and Discussion

This study investigates precipitation scaling rates (PSR) and factors affecting them at multiple locations in Canada. In particular the variation of PSR with reference to extreme precipitation selection approaches, precipitation durations, seasons, and distance from large waterbodies is

**Table 5** Precipitation scaling rates obtained in wintertime at locations away from large waterbodies

| Station | Method | 5m | 10m | 15m | 30m | 1h | 2h | 6h | 12h | 24h |
|---|---|---|---|---|---|---|---|---|---|---|
| BRN | a-max | -4.0 | -4.2 | -6.0 | -8.0 | -4.6 | -4.3 | -9.8 | -8.9 | 2.6 |
| | q80 | 0.6 | -1.7 | 0.2 | 0.1 | -1.6 | 1.4 | 2.3 | 0.8 | 1.1 |
| | q85 | 0.6 | -1.9 | -1.5 | -0.1 | 0 | 3.7 | -1.4 | 0.4 | -0.2 |
| | q90 | 1.6 | 1.2 | -0.9 | -0.9 | 0.9 | 1.6 | 1.8 | 2.1 | 0.2 |
| | q95 | 1.5 | 1.4 | 4.4 | 1.5 | 1.7 | -4.5 | -6.6 | -6.4 | -0.9 |
| | q97 | 2.4 | 1.4 | 2.9 | 1.2 | -0.8 | -2.3 | 0.5 | -0.8 | 0.8 |
| | q98 | 2.4 | 0.6 | 2.1 | -0.4 | -0.8 | -2.9 | -0.1 | -1.4 | -0.5 |
| | q99 | 0 | 0 | 0 | 0.1 | 0.1 | 0 | 0.1 | 0.2 | -0.1 |
| KIN | a-max | 1.6 | 0.9 | -1.1 | -4.0 | -0.4 | -0.1 | 0.7 | -9.9 | -5.6 |
| | q80 | -0.2 | 3.1* | 0.6 | 1.4 | 0.5 | 1.4 | 0.7 | -0.7 | -0.6 |
| | q85 | -0.2 | 1.0 | 0.6 | 1.4 | 0.8 | 0.2 | -4.2 | -1.2 | -0.3 |
| | q90 | -2.1 | 0.7 | 0 | 0.4 | 1.0 | 0.1 | -3.1 | 2.9 | 1.4 |
| | q95 | 2.1 | -0.9 | -0.9 | -2.7 | 1.7 | -3.2 | -0.5 | -0.7 | -3.0 |
| | q97 | 1.9 | 1.3 | 0 | 2.4 | 0.1 | 4.7 | 2.3 | -0.1 | 0.5 |
| | q98 | 0.1 | -0.1 | -0.2 | -0.5 | -0.4 | 0.3 | 1.1 | 0.7 | -0.1 |
| | q99 | -0.1 | 0 | 0.1 | 0.6 | 0.1 | -0.4 | 0.2 | 0.2 | -0.2 |
| IND | a-max | 4.0 | 3.5 | 3.2 | -0.1 | 4.1 | 1.9 | 2.5 | 2.1 | -0.4 |
| | q80 | 0.1 | -2.2 | -2.4 | 1.7 | 0.7 | -2.6 | 2.8 | 2.2 | 2.4 |
| | q85 | 0.1 | -1.6 | -3.3 | 0.9 | -0.3 | -3.3 | 1.6 | -0.4 | 3.1 |
| | q90 | 0.1 | -1.4 | -2.0 | -1.2 | -0.7 | -2.3 | 1.5 | 2.3 | 2.6 |
| | q95 | 3.6 | 0 | -2.0 | 0 | -0.1 | -1.6 | 0.1 | -2.8 | 2.5 |
| | q97 | 0.1 | 0 | 0.6 | -0.5 | 0.5 | -0.2 | -0.2 | -0.6 | 4.4 |
| | q98 | 0.5 | 0.1 | -0.4 | -0.1 | -0.2 | 0.5 | 0.6 | -1.1 | 1.3 |
| | q99 | 0.4 | -0.3 | -0.1 | 0.4 | -0.6 | -0.1 | 0.8 | -0.8 | 0.2 |
| WEY | a-max | 1.5 | 0.9 | 0.4 | 3.1 | 3.9 | 3.1 | 3.1 | 2.6 | 1.8 |
| | q80 | -0.3 | -0.5 | 0 | -1.2 | 0.5 | 0.8 | 0.7 | -2.1 | 1.7 |
| | q85 | -0.6 | -0.2 | -0.4 | -1.2 | 2.1 | 3.1* | 2.1 | 0.5 | 1.5 |
| | q90 | -0.6 | 0.5 | -0.3 | 0.4 | 1.8 | 2.8 | 0.8 | 2.1 | 0.5 |
| | q95 | 0.7 | 1.4 | 0.9 | -0.9 | -2.1 | -2.6 | 1.4 | 2.3 | 1.7 |
| | q97 | 0.5 | 4.5 | 1.2 | 1.1 | -0.6 | 2.7 | 1.9 | 2.0 | -0.2 |
| | q98 | 1.1 | 6.4 | 0.4 | 0.8 | -0.5 | 0.6 | -1.1 | 0.5 | 6.2 |
| | q99 | -0.6 | -0.5 | -0.1 | 0.8 | -0.4 | -0.1 | 0.4 | -2.2 | -6.5 |

Statistically significant scaling rates (at $p = 0.05$) are marked with an asterisk (*) sign. Cells filled with dark and light blue (orange) colors are associated with statistically significant and statistically insignificant positive (negative) scaling rates respectively

investigated. The novelty of this study is one of the few studies that have assessed observed PSR magnitudes in Canada. Furthermore, trend based approach as recommended in Zhang et al. (2017a) have been used to calculate PSR magnitudes as opposed to temperature-bin approach commonly used in previous studies.

The magnitude of observed precipitation scaling rates are calculated following the Clausius-Clapeyron relationship which conveys that natural logarithm of the magnitude of precipitation extremes vary linearly with temperature. Results indicate that in the summertime, precipitation extremes have drastically intensified at these locations with increasing temperatures. The intensification is more drastic for shorter duration precipitation events at locations away from large waterbodies than for longer duration events at locations near large waterbodies. Wintertime precipitation, on the other hand, has increased at a rate lower

than the summertime precipitation at these locations. The intensification is again found to be more drastic for shorter duration precipitation events than for longer duration precipitation events but more intense at locations near large waterbodies than locations away from large waterbodies.

More drastic intensification of shorter duration events is expected because shorter duration events require lesser amounts of moisture supply to intensify than longer duration events. Above results indicate that locations away from large waterbodies are most at risk of increases in convection driven summertime extreme precipitation in a warmer future climate. On the other hand, locations closer to large waterbodies are most at risk of increases in wintertime extreme precipitation in a warmer future climate.

The magnitude and statistical significance of precipitation scaling rates are found to vary considerably with the choice of extreme precipitation selection method. The scaling rates are also found to be considerably lower than the theoretical precipitation scaling rate of 7% per °C identified in the literature. These results verify C-C relationship i.e. there exist a relationship between precipitation extremes magnitude and temperature. However, they also highlight that this relationship is highly complex in nature and that PSR can deviate considerably from the theoretical precipitation scaling rate depending on some of the factors investigated in this study.

The results presented and discussed in this study are based on the assessment performed at representative locations in Canada and the conclusions should not be generalized to all locations in Canada or around the globe. Analysis presented in this study can be extended to other locations to further validate the findings made in this study. Availability of publically available, continuous, high temporal frequency precipitation observations would be vital to extend this analysis to other locations. Regard that PSR magnitudes calculated in this assessment are values averaged across different phases of the internal variability of climate. Future studies interested in assessing the effects of internal variability of climate on PSRs can extend this analysis to only include time-periods when specific modes of internal climate variability such as El Niño–Southern Oscillation (ENSO) are active.

Regardless of above limitations, the analysis does offer useful insights into the spatio-temporal variability of PSRs at the analyzed locations which can help in improving our current understanding and forecasting abilities of precipitation extremes under global warming.

**Acknowledgements** We are thankful to Environment Canada and especially Dr. Ka-Hing Yau and Dr. Xuebin Zhang for providing us with 5 min precipitation data for the locations analyzed in the study. Funding for the presented research has been provided by Natural Science and Engineering Research Council (NSERC) of Canada discovery grant to the third author.

## References

Berg P, Haerter JO (2013) Unexpected increase in precipitation intensity with temperature – A result of mixing of precipitation types? Atmos Res 119:56–61

Berg P, Haerter JO, Thejll P, Piani C, Hagemann S, Christensen JH (2009) Seasonal characteristics of the relationship between daily precipitation intensity and surface temperature. J Geophys Res 114: D18102

Drobinski P, Silva ND, Panthou G, Bastin S, Muller C, Ahrens B, Borga M, Conte D, Fosser G, Giorgi F, Guttler I, Kotroni I, Li L, Morin E, Onol B, Quintana-Segui P, Romera R, Torma CZ (2016) Scaling precipitation extremes with temperature in the Mediterranean: past climate assessment and projection in anthropogenic scenarios. Clim Dyn. https://doi.org/10.1007/s00382-016-3083-x

Haerter JO, Berg P, Hagemann S (2010) Heavy rain intensity distributions on varying time scales and at different temperatures. J Geophys Res 115:D17102

Koenker R, Kevin FH (2001) Quantile Regression. J Econ Perspect 15(4):143–156

Lenderink G, Meijgaard EV (2008) Increase in hourly precipitation extremes beyond expectations from temperature changes. Nat Geosci 1:511–514

Miao C, Sun Q, Borthwick AGL, Duan D (2016) Linkage Between Hourly Precipitation Events and Atmospheric Temperature Changes over China during the Warm Season. Sci Rep 6:22543. https://doi.org/10.1038/srep22543

Molnar P, Fatichi S, Gaal L, Szolgay J, Burlando P (2015) Storm type effects on super Clausius–Clapeyron scaling of intense rainstorm properties with air temperature. Hydrol Earth Syst Sci 19:1753–1766. https://doi.org/10.5194/hess-19-1753-2015

Panthou G, Mailhot A, Laurence E, Talbot G (2014) Relationship between Surface Temperature and Extreme Rainfalls: A Multi-Time-Scale and Event-Based Analysis. J Hydrometeorol 15:1999–2010. https://doi.org/10.1175/JHM-D-14-0020.1

Scoccimarro E, Villarini G, Vichi M, Zampieri M, Fogli PG, Bellucci A, Gualdi S (2015) Projected changes in intense precipitation over Europe at the daily and subdaily time Scales. J Clim 28(15):6193–6203

Shaw SB, Royem AA, Riha S (2011) The Relationship between Extreme Hourly Precipitation and Surface Temperature in Different Hydroclimatic Regions of the United States. J Hydrometeorol 12:319–325

Stocker TF, Qin D, Plattner G-K, Alexander LV, Allen SK, Bindoff NL, Bréon F-M, Church JA, Cubasch U, Emori S, Forster P, Friedlingstein P, Gillett N, Gregory JM, Hartmann DL, Jansen E, Kirtman B, Knutti R, Kumar KK, Lemke P, Marotzke J, Masson-Delmotte V, Meehl GA, Mokhov II, Piao S, Ramaswamy V, Randall D, Rhein M, Rojas M, Sabine C, Shindell D, Talley LD, Vaughan DG, Xie S-P (2013) Technical summary. In: Stocker TF, Qin D, Plattner G-K, Tignor M, Allen SK, Boschung J, Nauels A, Xia Y, Bex V, Midgley PM (eds) Climate change 2013: the physical science basis. Contribution of working group I to the fifth assessment report of the intergovernmental panel on climate change. Cambridge University Press, Cambridge and New York

Wasko C, Sharma A (2014) Quantile regression for investigating scaling of extreme precipitation with temperature. Water Resour Res 50:3608–3614

Wasko C, Sharma A, Westra S (2016) Reduced spatial extent of extreme storms at higher temperatures. Geophys Res Lett 43:4026–4032. https://doi.org/10.1002/2016GL068509

Westra S, Alexander LV, Zwiers FW (2013) Global increasing trends in annual maximum daily precipitation. J Clim 26:3904–3918

Westra S, Fowler HJ, Evans JP, Alexander LV, Berg P, Johnson F, Kendon EJ, Lenderink G, Roberts NM (2014) Future changes to the intensity and frequency of shortduration extreme rainfall. Rev Geophys 52:522–555

Zhang X, Zwiers FW, Li G, Wan H, Cannon AJ (2017a) Complexity in estimating past and future extreme short-duration rainfall. Nat Geosci. https://doi.org/10.1038/ngeo2911

Zhang W, Villarini G, Scoccimarro E, Vecchi GA (2017b) Stronger influences of increased CO2 on subdaily precipitation extremes than at the daily scale. Geophys Res Lett 44:7464–7471